INTERFACE SCIENCE 10, 75–81, 2002

Finite Element Analysis of $CoSi_2$ Nanocrystals on Si(001)

I. GOLDFARB*, L. BANKS-SILLS AND R. ELIASI
Department of Solid Mechanics, Materials and Systems, The Fleischman Faculty of Engineering, Tel Aviv University, Ramat Aviv 69978, Israel
ilang@eng.tau.ac.il
http://www.eng.tau.ac.il/∼ilang

G.A.D. BRIGGS
Department of Materials, University of Oxford, Parks Road, Oxford OX1 3PH, UK

Abstract. In this work we present a finite element analysis of pyramidal and hut-shaped $CoSi_2$ nanocrystals reactively deposited onto Si(001) substrates. These dots have been observed by us, as well as by other groups. Our analyses have yielded four major conclusions: (1) Elastic relaxation of $CoSi_2$/Si mismatch strain by three-dimensional islands drives their nucleation, rendering flat, two-dimensional, layer energetically unfavourable. (2) The effect of the nanocrystal surface and interface energies for the observed vertical aspect ratios is negligible at small nanocrystal volumes. (3) Pyramids and huts with identical vertical aspect ratios are energetically degenerate. (4) Nanocrystal growth is only energetically favourable if accompanied by an increase in vertical aspect ratio. Most of these conclusions are consistent with those found in compressively strained layers, such as $Si_{1-x}Ge_x$ layers on Si.

Keywords: epitaxial cobalt silicide nanocrystals, scanning tunneling microscopy, finite element analysis, elastic and surface and interface energies, strain relaxation

1. Introduction

Cobalt disilicide ($CoSi_2$) is important as self-aligned contact and interconnect material, as well as for metal-based transistors and detectors [1]. High-quality, smooth epitaxial silicide layers could yield numerous advantages for such applications, especially on the preferred Si(001) surface. However, precisely on this surface three-dimensional (3D) islands result instead, whether in reactive or molecular beam epitaxy [2, 3], which may still be advantageous for applications in devices based on self-assembled quantum dots. This phenomenon is somewhat surprising, since 3D growth (which can be shown to be stabilized by the relaxation of mismatch strain by the 3D islands) is expected only at larger than 1.2% mismatch (that exists at the $CoSi_2$/Si interface) values [4]. If the 3D islands nevertheless nucleate, they are expected to form very large square-base pyramids, rather than the observed small and elongated huts [2, 3], as: (a) the island volume is inversely proportional to the sixth power of the mismatch strain and, (b) the square-base pyramid has been shown to comprise the lowest-energy configuration (at least up to a certain critical volume) [4, 5]. In fact, applying the linear elasticity formalism developed by Tersoff and co-workers for Ge/Si [4, 5], Brongersma et al. have shown that a critical size for the shape transition of $CoSi_2$ islands is almost 200 nm base-length [6].

Understanding the self-assembled and self-organized formation of nanocrystal arrays is not only scientifically challenging, but is paramount to their technological exploitation in future nano-electro-opto-mechanical applications. The pioneering application of the continuum elasticity theory to self-assembled

*To whom all correspondence should be addressed.

nanocrystals by Tersoff and co-workers [4, 5] has been undoubtedly validated (e.g. see Ref. [7]) and used by many groups, whether in analytical form [4, 5], or using numerical techniques, such as Green's functions [8] and the finite element (FE) method [9–15]. Unfortunately, most of these FE investigations have been performed almost exclusively on the compressively-strained $Si_{1-x}Ge_x$/Si islands.

In this work, we show, for the first time, a FE analysis that accounts for our growth and scanning tunneling microscopy (STM) observations of the tensile-strained $CoSi_2$ nanocrystals on the Si(001) surface.

2. Experimental Procedures

To grow $CoSi_2$ we used a reactive deposition epitaxy (RDE) process, where the Co is deposited from a precise e-beam evaporator onto a Si substrate at 500°C mounted in the elevated-temperature ultra-high vacuum (UHV, 10^{-8} Pa) STM stage (JEOL 4500-XT), *while scanning*, as described in previous publications [3, 16, 17]. Thereafter the evaporated Co atoms land and react with Si atoms from the substrate to create $CoSi_2$, while the process is being continuously monitored with an STM. This allows for the most intimate insight into the processes of nucleation and subsequent evolution of the 3D nanocrystals. The growth was terminated immediately after the appearance of a dense nanocluster array, as shown in Fig. 1(a).

3. Finite Element Analysis

To obtain the stress and strain fields for a cobalt disilicide layer or nanocrystal on a silicon substrate, a fictitious isotropic temperature gradient ΔT is imposed on the disilicide to create a mismatch strain ε_m. The actual strain arises from the atomic spacing (lattice constant) mismatch between the fluorite disilicide and the diamond silicon structures, and is given by:

$$\varepsilon_m = \frac{d_s - d_i}{d_i} \tag{1}$$

where d_i is the lattice constant of the island material and d_s of the substrate material. The mismatch strain in this case is $\varepsilon_m = 0.0125$. $CoSi_2$ is a cubic (fluorite) material with elastic stiffness constants $C_{11} = 228$ GPa, $C_{12} = 138$ GPa and $C_{44} = 94$ GPa [18]. The mechanical properties of Si (in an isotropic approximation)

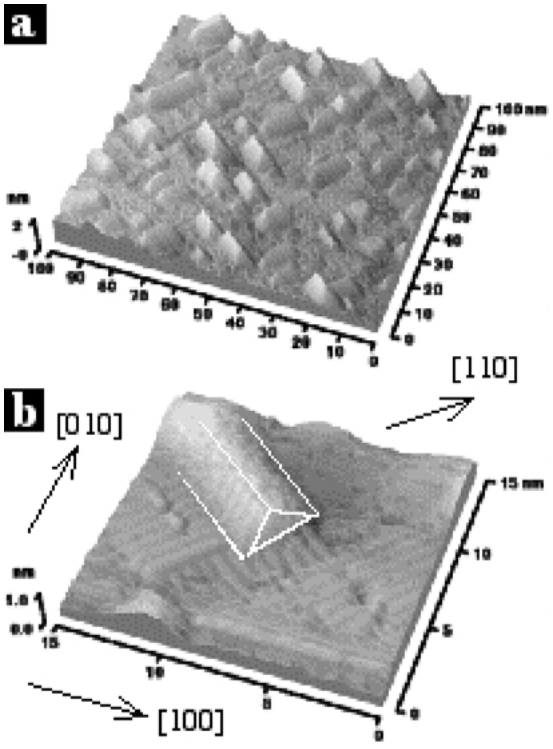

Figure 1. STM micrographs taken in real time during solid-phase epitaxy of $CoSi_2$ nanocrystals on a Si(001) substrate: (a) large field of view (100 nm × 100 nm × 2 nm) (b) one magnified nanocrystal (15 nm × 15 nm × 1 nm).

are Young's modulus $E = 131$ GPa and Poisson's ratio $\nu = 0.278$ [19].

For the 2D $CoSi_2$ layer, the mechanical energy caused by the atomic mismatch may be obtained numerically, or analytically. The elastic energy of a flat continuous film of volume V, U_{el} , is given by [20]:

$$U_{el} = \frac{(C_{11} + 2C_{12})(C_{11} - C_{12})}{C_{11}} \varepsilon_m^2 V \tag{2}$$

For the $CoSi_2$ island on a silicon substrate, a finite element analysis is carried out using the commercial finite element program ADINA [21], with a mesh consisting of 10140 twenty-noded, three-dimensional isoparametric elements and 44828 nodal points, as shown in Fig. 2. As noted, a temperature change $\Delta T = 1$°C is applied. The stress is given by:

$$\sigma_{ij} = C_{ijkl}\varepsilon_{kl} - \beta_{ij}\Delta T \tag{3}$$

where C_{ijkl} is the stiffness matrix, ε_{ij} is the strain tensor, $\beta_{ij} = \alpha C_{ijkl}$, and the coefficient of thermal

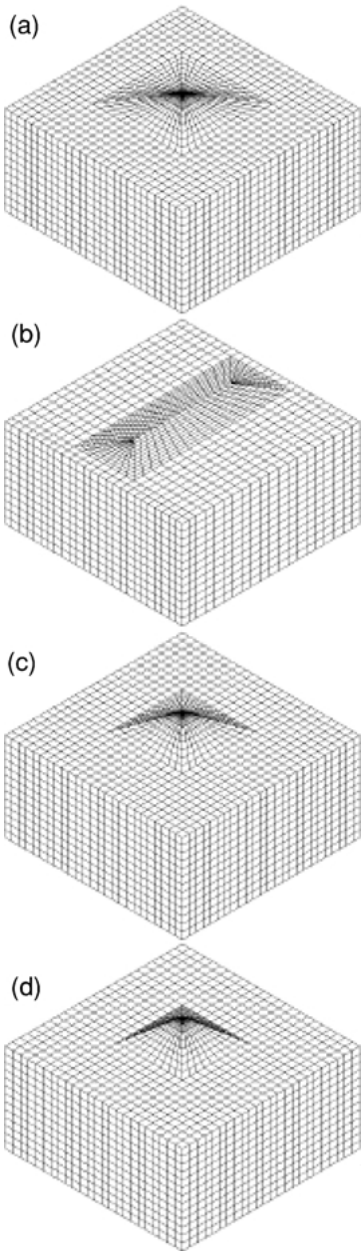

Figure 2. Finite element modelling of $CoSi_2$ nanocrystals on a Si(001) substrate. (a) nanocluster "2" (vertical aspect ratio 0.15), (b) hut (vertical aspect ratio 0.15), (c) "4" (vertical aspect ratio 0.28), and (d) "5" (vertical aspect ratio 0.39). The volume of each nanocrystal is 52 nm^3. In this and subsequent figures, the numbers "1" through "6" designate increasing nanocrystal size (see text for details).

expansion α is taken to be ε_m. The strain energy density W is that of the mechanical energy only, so that [22]:

$$W = \frac{1}{2}\varepsilon_{ij}^{m}\,\sigma_{ij} \tag{4}$$

where

$$\varepsilon_{ij}^{m} = \varepsilon_{ij} - \varepsilon_m \delta_{ij}\Delta T \tag{5}$$

and δ_{ij} is the Kronecker delta. Thus the strain energy for the island and substrate is given by:

$$U_{i+s} = \int_{V_i+V_s} W\,dV \tag{6}$$

where V_i and V_s are the volume of the island and the substrate, respectively. In the case of the flat 2D $CoSi_2$/Si layer the strain in the Si substrate is zero, and so is the strain energy in the substrate. The nanocrystal island, on the other hand, induces a strain field in the substrate and hence, the strain energy density in the substrate is non-zero.

4. Total Energy Calculations

The total energy expression must also include the surface and interface energy terms. For the flat $CoSi_2$ layer:

$$E_{2D}^{total} = U_{el} + \Gamma_{int} + \Gamma_{surf} \tag{7}$$

where Γ_{int} and Γ_{surf} are the respective $CoSi_2$/Si interface and the outer $CoSi_2$ layer surface energies defined as (Γ) = surface energy density $(\gamma)\times$ surface area (A). For the three-dimensional $CoSi_2$ nanoisland:

$$E_{3D}^{total} = U_{i+s} + \Gamma_{int} + \Gamma_{facet} \tag{8}$$

where Γ_{int} and Γ_{facet} are the $CoSi_2$/Si interface and $CoSi_2$ nanocrystal facet energies.

Surface and interface energies are the most problematic terms in expressions (7) and (8), because the surface energy densities, γ, are rarely known, particularly for the $CoSi_2$/Si case. Moreover, while the interface between $CoSi_2$ and Si can be flat [23, 24], multiple-faceted interfaces have also been reported [25, 26], which further complicates the derivation of the interface energy. For example, Adams et al. using a reverse Wulf approach could only obtain a relative quantity for the $CoSi_2$/Si interface along {111} and {100} facets, in the form of a ratio with $\gamma_{\{100\}}/\gamma_{\{111\}} = 1.43$ [26]. Even theoretical estimations exist only for certain surfaces, e.g. $CoSi_2${110}, and interfaces, e.g. $CoSi_2${100}/Si{100} and $CoSi_2${111}/Si{111} [18, 27–29]. Most of the $CoSi_2$ nanocrystals in this study, such

as the ones shown in Fig. 1, were found to be {221}-oriented, having mixed facets of the {111} and {110} type [3].

Based on this data, the surface and interface energy terms were employed as free parameters, ranging from the lowest to the highest possible value within reasonable limits: $0.50\ \text{J/m}^2 \leq \gamma_{\text{int}} \leq 2.50\ \text{J/m}^2$ and $1.00\ \text{J/m}^2 \leq (\gamma_{\text{facet}} = \gamma_{\text{surf}}) \leq 3.00\ \text{J/m}^2$.

5. Results and Discussion

In order to model the experimentally observed $CoSi_2$ nanocrystal arrays on the Si(001) surface, such as shown in Fig. 1(a), we first measured the average inter-nanocrystal distances from this and similar STM micrographs, to determine an average portion of the substrate occupied by a single $CoSi_2$ nanocrystal. This 400 nm^2 area was taken to be the limiting slab area, as shown in Fig. 2. The slab thickness was taken to be about ten times the nanocrystal height, i.e. 10 nm. The nanocrystal facets have been found by the authors to be of {111} and {110} orientations, forming angles of 15.3° and 18.9°, respectively, with the {221} base [3] (c.f. Fig. 1(b)). Lastly, the mean nanocrystal size found from the size distribution such as in Fig. 1(a) and other STM micrographs was used here.

Hence the simulated pyramid in Fig. 2(a) represents a square based $CoSi_2$ nanocrystal, with two out of four facets inclined 15.3°, and the remaining two 18.9°. Figure 2(b) models the more frequently observed shape of elongated huts, as in Fig. 1, (increased lateral aspect ratio (LAR)), while still maintaining the same facet inclinations (similar vertical aspect ratio (VAR)) and the same volume. LAR is defined as a long nanocrystal base-side length to the short base-side length ratio, and VAR as a nanocrystal height to the mean base-side length ratio. Figure 2(c) and (d) while maintaining the same volume as in 2(a) and (b) exhibit progressively increasing facet inclination and, hence, represent increasing VAR.

5.1. *The Effect of the Surface and Interface Energy Densities*

It is instructive to learn about the relative importance of the surface and interface energy densities in total energy calculations. We choose the ratio $E_{3D}^{\text{total}}/E_{2D}^{\text{total}}$ (see Eqs. (7) and (8)) as a criterion for the stability of the 3D nanocrystals relative to a flat 2D layer,

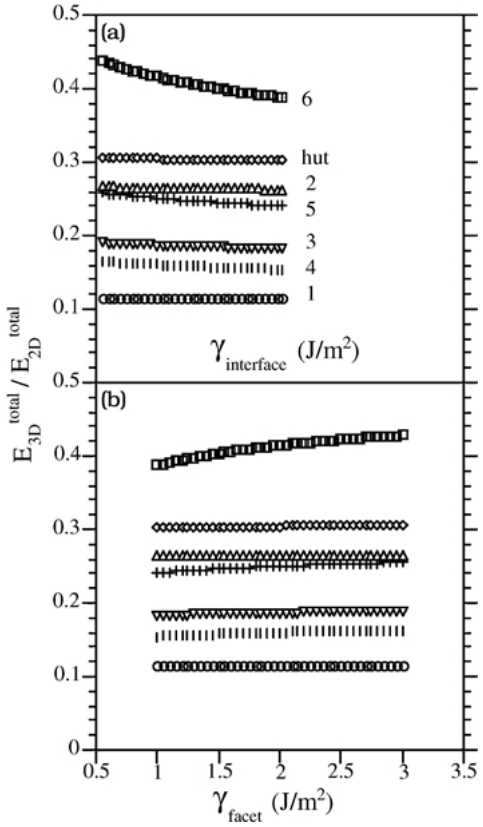

Figure 3. Dependence of the $E_{3D}^{\text{total}}/E_{2D}^{\text{total}}$ ratio on the interface, surface, and facet energy densities.

i.e. the smaller the $E_{3D}^{\text{total}}/E_{2D}^{\text{total}}$ ratio the more stable the nanocrystals are and the less stable the 2D layer is. As already mentioned in Section 4, we take the surface and interface contributions as parameters to cover all plausible energetic ranges. Fig. 3(a) shows the $(E_{3D}^{\text{total}}/E_{2D}^{\text{total}})$ dependence on the interface energy density, $0.50\ \text{J/m}^2 \leq \gamma_{\text{int}} \leq 2.00\ \text{J/m}^2$, when $\gamma_{\text{facet}} = \gamma_{\text{surf}} = 2.00\ \text{J/m}^2$, and 3(b) on the facet and surface energy densities, $1.00\ \text{J/m}^2 \leq (\gamma_{\text{facet}} = \gamma_{\text{surf}}) \leq 3.00\ \text{J/m}^2$, with $\gamma_{\text{int}} = 1.00\ \text{J/m}^2$.

The first obvious conclusion is that for small nanocrystal volumes the influence of the interface and facet energies is negligible. The volume increases when going from "1" (15 nm^3) to "6" (264 nm^3), with the "2", "hut", "3" and "4", shown in Fig. 2(a)–(d), respectively, having the same volume of 52 nm^3. Only at that largest nanocrystal volume of 264 nm^3 ("6"), both the surface and interface energy densities begin to significantly affect the stability, however in opposite directions. This can be understood in the light of our assumptions. We attributed the same energy for

the interface between the 3D nanocrystal and the substrate as for the interface between the 2D layer and the substrate. Hence, as the interface area in the 2D case is significantly larger than in the 3D case, higher interface energy density will raise the 2D interface energy term, Γ_{int} in Eq. (7), to a significantly higher level than the respective 3D interface energy term, Γ_{int} in Eq. (8). This will, in turn, cause the $E_{3D}^{total}/E_{2D}^{total}$ ratio to slightly decrease with increasing interface energy density, as in Fig. 3(a), as a manifestation of an increased nanocrystal stability. The situation is reversed, when the surface and facet energy density terms are considered, because of the larger surface area of the nanocrystal relative to the flat layer case, thus accounting for an increasing $E_{3D}^{total}/E_{2D}^{total}$ ratio (with increasing surface and facet energy terms) and relative 2D layer stabilisation.

5.2. *The Nanocrystal Island Volume Effect*

Next, we were interested in understanding the driving force (if there was any) for further growth of the nanocrystal embrios after their nucleation. Understanding of growth and coarsening is paramount, as these processes determine the nanocrystal suitability for the creation of quantum dot arrays. For example, if there is a large driving force for the nanocrystals to coarsen and coalesce, it may prove very difficult to produce and maintain arrays of small and uniformly shaped dots. Figures 4(a) and 5(a) show the dependence of the elastic, as well as total, energy on the nanocrystal volume for two discrete cases: Fig. 4(a), with $\gamma_{int} = 0.55$ J/m^2 and $\gamma_{facet} = \gamma_{surf} = 4.00$ J/m^2, and Fig. 5(a) where $\gamma_{int} = \gamma_{facet} = \gamma_{surf} = 2.00$ J/m^2. These values do not significantly affect the total energy of nanocrystals with volumes smaller than 260 nm^3 (see Fig. 3).

Two important conclusions are immediately evident:

I. reduction of the elastic strain energy, U_{i+s}, stored in the deposit always favours the *formation and growth* of 3D nanocrystals, however
II. increasing the nanocrystal island volume *raises* the total system energy, E_{3D}^{total}, thus stabilising 2D morphology, provided that VAR does not vary.

5.3. *The Vertical (VAR) and Lateral (LAR) Aspect Ratio Effect*

Johnson and Freund have found that, for a Ge/Si system, increasing VAR leads to a reduction of the total

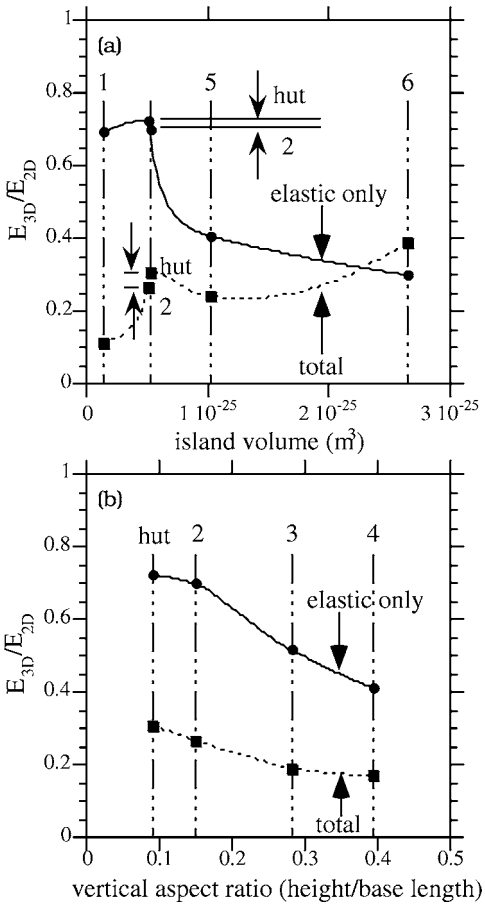

Figure 4. Dependence of the elastic strain energy ratio U_{i+s}/U_{el} from expressions (2) and (6) (filled circles connected by a continuous line to guide the eye) and total energy ratio $E_{3D}^{total}/E_{2D}^{total}$ from expressions (7) and (8) (filled squares connected by a dotted line to guide the eye) on the (a) nanocrystal volume and (b) vertical aspect ratio, for the arbitrary chosen surface and interface energy density values, $\gamma_{int} = 0.55$ J/m^2 and $\gamma_{facet} = \gamma_{surf} = 4.00$ J/m^2.

energy, provided the surface and interface energy terms are not too high [14]. A similar analysis for the $CoSi_2$/Si system was conducted here. The results are shown in Figs. 4(b) and 5(b). It appears that the results obtained in this study are in agreement with those for Ge/Si from Johnson and Freund; an increase in VAR reduces both the elastic strain energy and the *total* energy terms. This indicates that nanocrystal growth is only energetically favourable if the increase in the nanocrystal volume is followed by a respective increase in its VAR.

Another interesting observation is related to the nanocrystal island LAR. Analytical calculations by Tersoff et al. have shown that a square-based pyramid

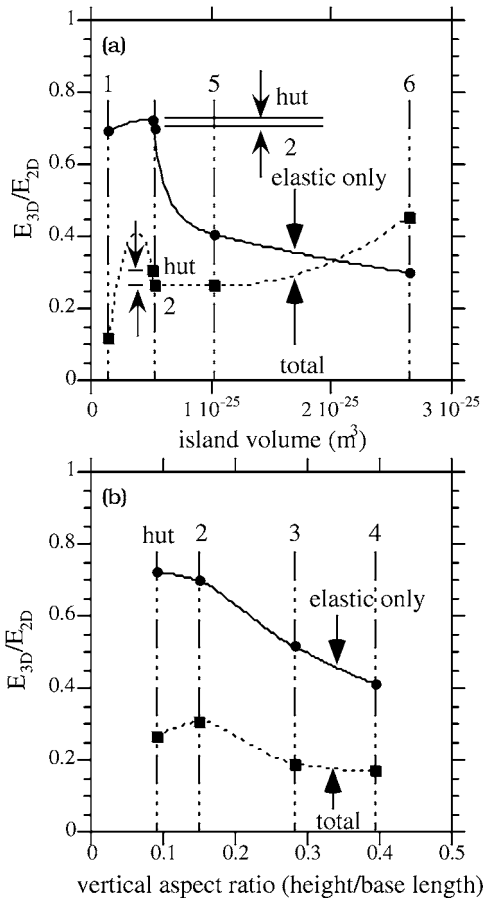

Figure 5. Dependence of the elastic strain energy ratio U_{i+s}/U_{el} from expressions (2) and (6) (filled circles connected by a continuous line to guide the eye) and total energy ratio $E_{3D}^{total}/E_{2D}^{total}$ from expressions (7) and (8) (filled squares connected by a dotted line to guide the eye) on the (a) nanocrystal volume and (b) vertical aspect ratio, for the arbitrary chosen surface and interface energy density values, $\gamma_{int} = \gamma_{facet} = \gamma_{surf} = 2.00$ J/m^2.

is the most energetically favourable shape, at least until some critical size is reached [4, 5], e.g. 180 nm in the $CoSi_2$/Si case [6]. However, our calculations show that hut-shaped and pyramidal nanocrystals (with almost identical and much smaller volumes) are nearly degenerate in energy (see how negligible is the energetic difference between "hut" and "2" in Figs. 4 and 5). This could account for the observed mostly elongated, small, hut-shaped Ge/Si [19] and $CoSi_2$/Si [2, 3, 16, and Fig. 1 in this work] nanocrystals, since any kinetic instability, such as the one proposed in Ref. [3], may cause the nanocrystals to elongate, at an almost negligible energetic cost.

6. Conclusions

In this investigation we have grown $CoSi_2$ nanocrystals on a Si(001) substrate, in the elevated-temperature UHV STM, and subsequently modelled them in the framework of continuum elasticity using finite element analysis. Based upon this analysis we were able to draw four basic conclusions.

1. Elastic relaxation is the driving force for nucleation of 3D nanocrystals, which is not possible in a flat 2D layer.
2. Surface and interface energy densities do not have a major impact on the total nanocrystal-substrate system energy, until relatively large nanocrystal volumes are reached.
3. Pyramids and huts that exhibit similar volumes and vertical aspect ratios, are, practically, degenerate in energy. That implies that a pyramidal nanocrystal nucleus can easily evolve into a hut by anisotropic elongation, e.g. due to certain kinetic constraints, almost without raising the total energy of the system.
4. Only if the nanocrystal growth is accompanied by a respective increase in the vertical aspect ratio, will such growth be energetically favourable.

References

1. S.P. Murarka, *Silicides for VLSI Applications* (Academic Press, New York, 1983).
2. V. Scheuch, B. Voigtländer, and H.P. Bonzel, Surf. Sci. **372**, 71 (1997).
3. I. Goldfarb and G.A.D. Briggs, Phys. Rev. B **60**, 4800 (1999).
4. J. Tersoff and F.K. LeGoues, Phys. Rev. Lett. **72**, 3570 (1993).
5. J. Tersoff and R.M. Tromp, Phys. Rev. Lett. **70**, 2782 (1993).
6. S.H. Brongersma, M.R. Castell, D.D. Perovic, and M. Zinke-Allmang, Phys. Rev. Lett. **80**, 3795 (1998).
7. J. Tersoff, Phys. Rev. Lett. **79**, 4934 (1997).
8. D.A. Faux and G.S. Pearson, Phys. Rev. B **62**, R4798 (2000).
9. S. Christiansen, M. Albrecht, H.P. Strunk, and H.J. Maier, Appl. Phys. Lett. **64**, 3617 (1994).
10. S. Christiansen, M. Albrecht, H.P. Strunk, P.O. Hansson, and E. Bauser, Appl. Phys. Lett. **66**, 574 (1995).
11. D.J. Eaglesham and R. Hull, Mat. Sci. Eng. B **30**, 197 (1995).
12. H.P. Strunk, M. Albrecht, S. Christiansen, and W. Dorsch, Inst. Phys. Conf. Ser. No. **157**, 323 (1997).
13. K. Tillman, B. Rahmati, H. Trinkaus, W. Jäger, A. Hartmann, R. Loo, L. Vescan, and K. Urban, Inst. Phys. Conf. Ser. No. **157**, 343 (1997).
14. H.T. Johnson and L.B. Freund, J. Appl. Phys. **81**, 6081 (1997).
15. Th. Wiebach, M. Schmidbauer, M. Hanke, H. Raidt, R. Kohler, and H. Wawra, Phys. Rev. B **61**, 5571 (2000).
16. I. Goldfarb and G.A.D. Briggs, Surf. Sci. **454–456**, 837 (2000).
17. I. Goldfarb and G.A.D. Briggs, J. Mater. Res. **16**, 744 (2001).

18. R. Stalder, W. Wolf, R. Podloucky, G. Kresse, J. Furthmüller, and J. Hafner, Phys. Rev. B **56**, 1729 (1996).
19. I. Goldfarb and G.A.D. Briggs, Recent Res. Devel. In Mat. Sci. **1**, 191 (1998).
20. D.J. Bottomley and P. Fons, J. Cryst. Growth **160**, 407 (1996).
21. K.J. Bathe, *ADINA—Automatic Dynamic, Incremental Nonlinear Analysis System*, Version 7.4 (2000), Adina Engineering, Inc. USA.
22. B.A. Boley and J.H. Weiner, *Theory of Thermal Stresses* (Wiley, New York, 1960), p. 263.
23. C.W.T. Bulle-Lieuwma, A.F. DE Jong, and D.E.W. Vandenhoudt, Phil. Mag. A **64**, 255 (1991).
24. V. Buschmann, L. Fedina, M. Rodewald, and G. Van Tendeloo, Phil. Mag. Lett. **77**, 147 (1998).
25. C.W.T. Bulle-Lieuwma, A.H. van Ommen, J. Hornstra, and C.N.A.M. Aussems, J. Appl. Phys. **71**, 2211 (1992).
26. D.P. Adams, S.M. Yalisove, and D.J. Eaglesham, J. Appl. Phys. **76**, 5190 (1994).
27. R. Stalder, R. Podloucky, G. Kresse, and J. Hafner, Phys. Rev. B **57**, 4088 (1998).
28. R. Stalder, D. Vogtenhuber, and R. Podloucky, Phys. Rev. B **60**, 17112 (1999).
29. R. Stalder and R. Podloucky, Phys. Rev. B **62**, 2209 (2000).